Sensors and Materials, Vol. 13, No. 6 (2001) 325–342
MYU Tokyo

S & M 0453

The Structure of an Underetched Convex Mask Corner Explained as the Evolution of a Saddlepoint Vertex

Jaap van Suchtelen[1,2] and Erik van Veenendaal[2]

[1]MESA+ Research Institute, University of Twente,
P.O. Box 217, 7500 AE Enschede, Netherlands
[2]RIM Dept. of Solid State Chemistry, University of Nijmegen,
Toernooiveld 1, 6525 ED Nijmegen, Netherlands

(Received September 1, 2000; accepted December 1, 2000)

Key words: anisotropic etching, convex mask corner, numerical simulation, kinematic wave theory

Anisotropic etching of masked silicon single crystal wafers is widely used in micromachining technology. In this paper it is argued that the structure evolving from an underetched convex mask corner can be perfectly understood and calculated by straightforward application of kinematic wave theory. Previous attempts to predict such structures failed because they were based on an algorithm that, although applicable to protruding and re-entrant vertices, is insufficient to describe saddlepoint vertices. It is important to realize that a convex mask corner is a disguised saddlepoint vertex. For the extended algorithm discussed in this paper, two principles are essential which are not generally recognized: 1) In 3D we have to distinguish protruding, re-entrant and saddletype point sources. The surface structure evolving from such a point source may contain one or more saddlepoint vertices. 2) Saddlepoint vertices can act as a (topological) velocity source. This behaviour can be recognized by the concurrence of more than three edges in the vertex. These new principles are applied to explain the structure of the underetched mask corner on a Si{100} wafer etched in potassium hydroxide (KOH). Under specific conditions, this structure includes three velocity source saddlepoint vertices, three ordinary saddlepoint vertices and four protruding vertices.

1. Introduction

Orientation-dependent wet-chemical etching of single crystals is widely used as a tool in the fabrication of micro-mechanical devices such as mechanical sensors, actuators, and micropumps. Usually these devices are fabricated on flat single-crystalline substrates that are partly covered by a polygonized protecting mask, by exposing it to the etchant. The evolution of the shape of the crystal surface during the anisotropic etch process is determined by surface kinetics, and therefore it can be described mathematically by the kinematic wave theory as originally developed by Frank[1] and Chernov.[2] Essentially, this theory is a continuum description of the evolution of nonplanar surfaces, which may be considered as a generalisation of Huygens' principle for the evolution of wavefronts for orientation-dependent advance velocity $R(\boldsymbol{n})$.[3] A basic procedure in this theory is the Gibbs-Wulff construction, which produces the shape evolving from a point nucleus and also the shape developing from an edge (2D) and a vertex (3D). Algorithms for the numerical simulation of etched shapes can be based on this construction. Input data are the mask shape, substrate orientation and the etch rate function $R(\boldsymbol{n})$.

This paper is concerned with a curious phenomenon associated with the anisotropic-etching technology which is, up to now, poorly understood: the contrast between the structures developed at convex and at concave mask corners. The structure developing from a concave corner consists of surfaces with minimum etch rate, in agreement with the 3D Gibbs-Wulff construction. This construction, for this special case, is a direct and simple generalisation of the 2D Gibbs-Wulff construction described in many textbooks, which is also the basis of the construction of the underetch profile at a straight mask edge. Consequently, both this 2D profile and the 3D structure at a concave mask corner can be computed numerically from the $R(\boldsymbol{n})$ function by a simple and straightforward algorithm, as described in the literature on this subject.[3–6]

In contrast, the structure developing from a convex mask corner, in many cases, has some complications. First of all, although there is not a sharp distinction, the structures sometimes appear to be more intricate than those developed from a concave corner, showing more edges and vertices. Figure 1 shows an example of such a structure: the underetched convex mask corner on a {100} silicon surface with mask edges along <110> directions, as etched in KOH. Secondly, the occurring surfaces do not correspond either to minimum or maximum etch-rate orientations. Finally, part of the vertices occurring in these structures can be meeting points between more than three edges. This difference is topologically distinctive, but as far as we are aware it has not been mentioned before as typical for convex mask corners. This observation alone is proof of the fact that such >3-edged vertices actually nucleate one or more new orientations, and as such it has been a clue to the development of the new algorithm.

In this paper we will consider the structures developing at convex mask corners by underetching and we will develop a computer-executable algorithm which predicts them, on the basis of kinematic wave theory. In doing so, we will emphasize principles rather than elaborate on mathematics. We proceed by the following steps:

1) We identify the concave mask corner as a disguised "protruding vertex", and the convex mask corner as a disguised "saddlepoint vertex" in the initial surface (section 3).

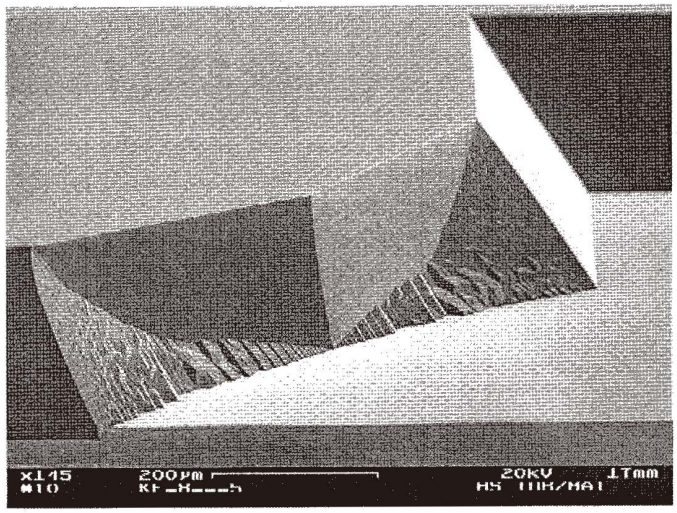

Fig. 1. AFM image of structure obtained by underetching a silicon (100) wafer below a convex mask corner. The mask edges are aligned in <110> and <10> directions and the anisotropic etchant is KOH (3 wt%, 80°C). Courtesy H. Schröder.

2) We discuss the evolution of vertices in general. First we consider the 2D case of the evolution of edges, as commonly explained in textbooks (section 4) and then transfer the method to the 3D case of vertices (section 5). We explain how the structure evolving from a saddlepoint vertex can be calculated in a single time step, by a new algorithm, which involves a sequence of calculations that reveal all vertices of the structure in succession. New generations of saddlepoint vertices may arise.

3) In section 6 we will apply these new principles to explain an obvious example of an underetched convex-mask corner structure which was investigated in detail by Schröder and Obermeier[7] and Schröder.[8]

To our knowledge it has been overlooked so far that the 3D case of a vertex is not simply a straightforward generalisation of the 2D case of an edge. This is due to the fact that a vertex defined by three planar sectors (the 3D generalisation of an edge defined by two half-infinite lines) can occur in three species: protruding, re-entrant and saddletype. The properties, and therefore the construction principles, of protruding and re-entrant edges and vertices correspond closely, but the saddletype vertex has no 2D analog. Although most authors seem to be aware of the extra complexity of the saddlepoint case,[3–5,7,9] a suitable algorithm has not been published so far. In a recent study,[9] we have analyzed the case in detail and developed a new and consistent construction procedure. Two new geometrical principles are involved in this procedure, which will be discussed in this paper on an intuitive level:

A) We argue that the character of a "point source" in this construction has to be specified. We have to distinguish between a convex and a concave point source, for the 2D

case of a protruding and a re-entrant edge, or for the 3D case of a protruding and a re-entrant vertex. For a saddlepoint vertex we have, by analogy, to deal with a saddletype point source. This implies that the surfaces which can occur in the developing structure are a priori restricted to those orientations which correspond with the appropriate similar saddletype parts of the "Gibbs-Wulff surface", derived from the $R(\boldsymbol{n})$ function (in our notation, the $\boldsymbol{QR}$ surface). This topological observation considerably reduces the complexity of the algorithm to be worked out for the numerical prediction.

B) We argue that moving saddlepoint vertices have the unique ability to nucleate new orientations - which, if they do, is reflected in the topological characteristic of more than three edges meeting in the vertex. We show that the "conical Gibbs-Wulff construction" (explained in the appendix and more extensively in Ref. 9) can predict the nucleated orientations and consequently can be developed into an extended algorithm for calculating the structure of the evolving saddlepoint vertex.

2. Notations and Conventions

The reader is assumed to be familiar with kinematic wave theory, which is standard textbook material in the fields of crystal growth and etching.[10-13] The point of departure of this geometrical description is the polar plot of the perpendicular advance rate $R(\boldsymbol{n})$, which can be defined in two as well as in three dimensions. Whereas R is a scalar property, the polar representation of R for a certain orientation $\boldsymbol{n}$ is a vector in velocity space which can be written as $\boldsymbol{n}R(\boldsymbol{n})$. For convenience we introduce the notation $\boldsymbol{P}R(\boldsymbol{n}) = \boldsymbol{n}R(\boldsymbol{n})$, where $\boldsymbol{P}$ is the "plotting operator".

The Gibbs-Wulff construction is based on the $\boldsymbol{P}R(\boldsymbol{n})$ curve (2D) or surface (3D) for all $\boldsymbol{n}$. At every point of this curve/surface, a line/plane perpendicular to $\boldsymbol{n}$ is drawn. The curve/surface tangent to all these lines/planes is called the Gibbs-Wulff curve/surface. It is easily shown that the vector on the Gibbs-Wulff curve/surface, corresponding with a normal vector $\boldsymbol{n}$, can be written as $\boldsymbol{Q}R(\boldsymbol{n}) = \boldsymbol{P}R(\boldsymbol{n}) + \mathrm{d}R(\boldsymbol{n})/\mathrm{d}\boldsymbol{n}$, where $\boldsymbol{Q}$ is introduced as another vector operator $\boldsymbol{Q} = \boldsymbol{I} + \mathrm{d}/\mathrm{d}\boldsymbol{n}$, working on a scalar function of orientation $\boldsymbol{n}$ ($\boldsymbol{I}$ = identity operator). We call it the Gibbs-Wulff operator. For a smoothly curved surface, an infinitesimal area with orientation $\boldsymbol{n}$ follows a kinematic wave trajectory with the vector velocity $\boldsymbol{Q}R(\boldsymbol{n})$.

We will use a special convention for the signs of edges and vertices. One of the basic lemmas of kinematic wave theory concerns the relationship between surviving orientations and the types of edges and vertices (protruding or re-entrant): in the evolution of a protruding edge/vertex, the slowest orientations survive (and, conversely, the fastest orientations survive in re-entrant edges/vertices). It is appropriate to choose a set of definitions in which the characteristic properties of the complementary types are identical in terms of growth and dissolution/etching conditions. To this end, we have to define the normal $\boldsymbol{n}$ of a surface to point in the direction in which the surface advances, rather than "from crystal to parent phase" as is perhaps more customary. This implies that if a certain edge on a crystal is protruding towards a parent phase or etching liquid, it is now called a protruding edge for the growth situation but a re-entrant edge for the etch situation. Simultaneously, the function $R(\boldsymbol{n})$ should be considered as positive for growth and dissolution alike.

Edges and vertices are in the first place defined by the orientations of the participating interfaces and in the second place by the sign of the edge(s) between them. Edges can occur in two species only, for which we introduce the following notation:

protruding edge: edge{$\boldsymbol{n}_1$ (+)$\boldsymbol{n}_2$}
re-entrant edge: edge{$\boldsymbol{n}_1$ (–)$\boldsymbol{n}_2$}.

The basic vertex has three interfaces with (different) orientations $\boldsymbol{n}_1$, $\boldsymbol{n}_2$ and $\boldsymbol{n}_3$ and occurs in eight species: protruding, re-entrant and six saddlepoint vertices, with the following notation (see Fig. 2):

protruding vertex: vertex{$\boldsymbol{n}_1$ (+)$\boldsymbol{n}_2$ (+)$\boldsymbol{n}_3$ (+)}	(no 1 in Fig. 2(a))
saddlepoint vertex: vertex{$\boldsymbol{n}_1$ (–)$\boldsymbol{n}_2$ (+)$\boldsymbol{n}_3$ (–)}	(no 2)
vertex{$\boldsymbol{n}_1$ (+)$\boldsymbol{n}_2$ (–)$\boldsymbol{n}_3$ (–)}	(no 3)
vertex{$\boldsymbol{n}_1$ (–)$\boldsymbol{n}_2$ (–)$\boldsymbol{n}_3$ (+)}	(no 4)
vertex{$\boldsymbol{n}_1$ (+)$\boldsymbol{n}_2$ (+)$\boldsymbol{n}_3$ (–)}	(no 5)
vertex{$\boldsymbol{n}_1$ (–)$\boldsymbol{n}_2$ (+)$\boldsymbol{n}_3$ (+)}	(no 6)
vertex{$\boldsymbol{n}_1$ (+)$\boldsymbol{n}_2$ (–)$\boldsymbol{n}_3$ (+)}	(no 7)
re-entrant vertex: vertex{$\boldsymbol{n}_1$ (–)$\boldsymbol{n}_2$ (–)$\boldsymbol{n}_3$(–)}	(no 8).

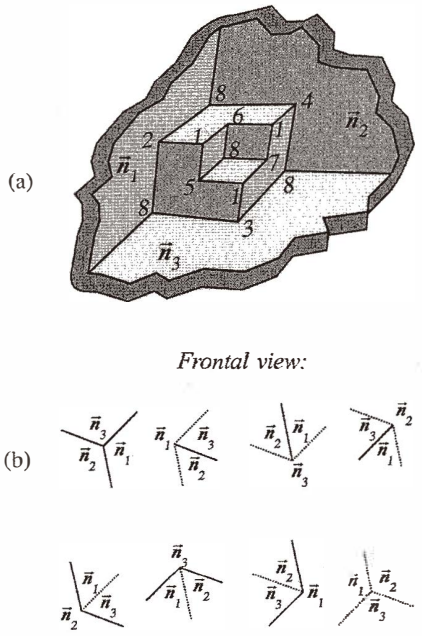

Fig. 2. Overview of the eight vertex types corresponding with three fixed orientations, $\boldsymbol{n}_1$, $\boldsymbol{n}_2$ and $\boldsymbol{n}_2$. a) Perspective view. b) Frontal view of the eight types as labeled in a.

The extension to vertices with more orientations is obvious. Note that the orientations $\boldsymbol{n}_1$, $\boldsymbol{n}_2$, *etc.* have to be numbered in cyclic order following a path around the vertex, but the direction of this path is irrelevant. The extension to an infinite number of orientations is a cone.

We have to emphasize that the word "edge" can actually be applied to two different objects, i.e., the actually 3D object of a folded planar sheet, i.e., two half-infinite planes connected by their intersection line, and the 2D object of two half-infinite lines connected by their intersection point. As far as the Gibbs-Wulff construction for their evolution is concerned, there is no difference: in the real 2D case we simply have one $\boldsymbol{n}$ variable in the $R(\boldsymbol{n})$ function, in the actual 3D case we are left with one $\boldsymbol{n}$ variable because it is restricted to the directions perpendicular to the edge line. For this reason we will not emphasize the difference in section 4. However, we may differentiate between the term point source in the strict 2D case and the term line source in the strict 3D case. However, an edge associated with a vertex is actually a half-infinite edge and the endpoint (i.e., the vertex) may move in a direction which is not perpendicular to it. The consequences are discussed in section 5.2.

In this paper we restrict ourselves to the simplest starting shapes: isolated edges and vertices defined by planar surfaces, which ensures that all occurring intersections are straight lines or half-lines. These starting shapes have the property that the evolving shape at any time after the start of the etching process can be calculated in a single time step. It can be rendered as a fixed shape in velocity space that simply has to be multiplied by the etching time to obtain the actual shape. We call this shape in velocity space the evolution shape of the edge or vertex surface. The surfaces and edges occurring in the evolution shape are not necessarily planar and straight, respectively.

We introduce some terminology concerning the relation between the starting shape of an edge or vertex (= the shape at time $t = 0$) and the evolution shape. If the shapes are identical, we call the edge or vertex persistent. In their respective 2D and 3D representations, the evolving edge or vertex point then follows a single straight trajectory so that we can define a vector velocity $\boldsymbol{R}_{\text{edge}}$ or $\boldsymbol{R}_{\text{vertex}}$ for it. If the shapes are not identical, this implies that beveling surfaces affect the evolution shape. For an edge this can only mean that it becomes truncated, so that the original edge point is cut off by the beveling surface and the original edge splits up into partial edges each following different trajectories, and/or (cylindrically) curved sections. These secondary edges are persistent. For a non-persistent edge or vertex we can still define the trajectory and the vertex velocity of the virtual edge or vertex, $\boldsymbol{R}(\boldsymbol{n}_1,\boldsymbol{n}_2)$ or $\boldsymbol{R}(\boldsymbol{n}_1,\boldsymbol{n}_2,\boldsymbol{n}_3)$. The virtual edge is defined as the intersection line of the infinite original planes $\boldsymbol{n}_1$ and $\boldsymbol{n}_2$ and the virtual vertex as the intersection point of the infinite original planes $\boldsymbol{n}_1$, $\boldsymbol{n}_2$ and $\boldsymbol{n}_3$, all travelling with the speed corresponding to the $R(\boldsymbol{n})$ function, and thus the connectivity relation

$$\boldsymbol{R}_{\text{edge/vertex}} \bullet \boldsymbol{n}_i = R(\boldsymbol{n}_i), \tag{1}$$

is obeyed for all participating interfaces. For an edge this implies that we can construct $\boldsymbol{R}(\boldsymbol{n}_1,\boldsymbol{n}_2)$ by drawing, in a polar plot of $R(\boldsymbol{n})$, a circle through the origin and points $\boldsymbol{P}R(\boldsymbol{n}_1)$ and $\boldsymbol{P}R(\boldsymbol{n}_2)$. $\boldsymbol{R}(\boldsymbol{n}_1,\boldsymbol{n}_2)$ is then the vector represented by the diameter of this circle from the

origin. The circle itself can be written as $\boldsymbol{P}\{\boldsymbol{R}(\boldsymbol{n}_1,\boldsymbol{n}_2)\bullet\boldsymbol{n}\}$. For a vertex formed by the three orientations $\boldsymbol{n}_1$, $\boldsymbol{n}_2$ and $\boldsymbol{n}_3$ we have the obvious extension of this principle by drawing a sphere through the origin and the points $\boldsymbol{PR}(\boldsymbol{n}_1)$, $\boldsymbol{PR}(\boldsymbol{n}_2)$ and $\boldsymbol{PR}(\boldsymbol{n}_3)$ (of course, the vector velocity of the vertex is the same for all eight vertex types). The sphere can be written as $\boldsymbol{P}\{\boldsymbol{R}(\boldsymbol{n}_1,\boldsymbol{n}_2,\boldsymbol{n}_3)\bullet\boldsymbol{n}\}$.

Whereas a beveling surface of an edge necessarily cuts off the original edge, so that the starting edge is not persistent, we have two alternative possibilities for the vertex case. The first possibility is that the original vertex point splits up into a number of secondary vertices, edges and/or curved areas. Again, such a structure as a whole is persistent: it can be represented as a fixed evolution shape in velocity space. A fortiori, secondary vertices on their own are persistent. The second possibility is that the beveling surface includes the vertex point itself. This implies that the vertex point as such is persistent (and also its vector velocity is identical to $\boldsymbol{R}(\boldsymbol{n}_1,\boldsymbol{n}_2,\boldsymbol{n}_3)$) but the vertex structure, being changed by the beveling plane, is not persistent. Obviously we have to distinguish between trajectory persistence and shape persistence for a vertex. Of course, shape persistence includes trajectory persistence, but not inversely.

3. The Correspondence between a Mask Corner and a Vertex

Shaw[12] and Jaccodine[13] describe a method for constructing underetch shapes. The evolution for the 2D case is predicted by considering the evolution of a 180° (= infinitely sharp) edge coinciding with the exposed surface, so that the edge line corresponds with the straight mask edge (Fig. 3(a)). Subsequently, the evolved shape, calculated on the basis of

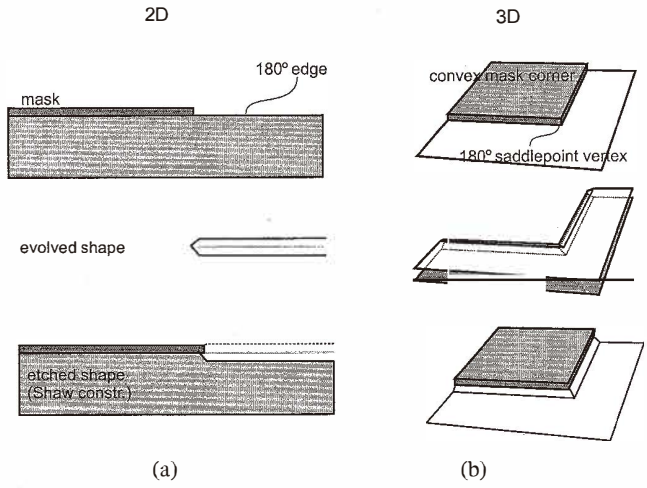

Fig. 3. Illustrating the formal identification of the situation at a mask edge with an evolving 180° edge (2D) and at a convex mask corner with a 180° saddlepoint vertex (3D).

the protruding edge evolution method that will be presented in section 4, is cut off by the mask which is considered as a boundary above which the shape is nonphysical. Note that, in a sense, this principle is simplistic as it assumes that the mask does not interact with the interface. In reality there may be an interaction, either resulting in an imposed orientation or in an enhanced nucleation rate. Such an interaction may provoke the mask junction to act as a velocity source.[14–16] We may generalize the 2D mask edge case to the 3D mask corner case by following the 180° edge around that corner (Fig. 3(b)). In both the 2D and the 3D cases, the choice for the 180° edge guarantees that any contact angle with the mask is possible. Note that a convex mask corner, both for the case of underetching and for overgrowth, corresponds to a saddlepoint vertex. Conversely, a concave mask corresponds to a protruding vertex.

The somewhat surprising consequence of this correspondence between mask corner types and vertex types is that, for the case of a masked planar substrate, re-entrant vertices simply never occur in the initial crystal surface. They may appear later, due to meeting events between convex vertices or edges with one another or with opposing planes. This happens when a masked area becomes underetched. Also, when etched surfaces originating from different mask openings or from opposed wafer sides meet, new saddlepoint vertices may be formed at the meeting point.

4. The 2D Case: Evolution of Protruding and Re-entrant Edges

Two fixed orientations, $\boldsymbol{n}_1$ and $\boldsymbol{n}_2$ ($\boldsymbol{n}_1 \neq \boldsymbol{n}_2$), define the complementary protruding and re-entrant starting edges $\{\boldsymbol{n}_1 (+)\boldsymbol{n}_2\}$ and $\{\boldsymbol{n}_1 (-)\boldsymbol{n}_2\}$. We choose a demo function $R(\boldsymbol{n})$ for which $\boldsymbol{PR}$ and $\boldsymbol{QR}$ are sketched in Fig. 4(a) in the relevant orientation range between $\boldsymbol{n}_1$ and $\boldsymbol{n}_2$. In Figs. 4(b) and 4(c), the transverse cross section of the starting edges is drawn with the edge position in the origin (protruding case in Fig. 4(b), re-entrant case in Fig. 4(c)).

After unit time, the two legs are displaced by the vectors $\boldsymbol{QR}(\boldsymbol{n}_1)$ and $\boldsymbol{QR}(\boldsymbol{n}_2)$, respectively, and the evolved shape is completed by connecting the points $\boldsymbol{QR}(\boldsymbol{n}_1)$ and $\boldsymbol{QR}(\boldsymbol{n}_2)$ following the curve $\boldsymbol{QR}(\boldsymbol{n})$ from $\boldsymbol{n}_1$ to $\boldsymbol{n}_2$ in the plane through $\boldsymbol{n}_1$ and $\boldsymbol{n}_2$. In this curve, self-intersections may occur (we have chosen $R(\boldsymbol{n})$ in order to produce such self-intersections for both cases, Figs. 4(b) and 4(c)). The "ears", cut short by the self-intersections, are nonphysical and should be eliminated. For a protruding edge (Fig. 4(b)) this applies to relatively faster orientations and for a re-entrant edge (Fig. 4(c)) to slower orientations. The shape after elimination of the ears is the shape obtained on the basis of the $R(\boldsymbol{n})$ function alone. In the following, we will refer to these shapes by $C(\boldsymbol{n}_1 (+)\boldsymbol{n}_2)$ and $C(\boldsymbol{n}_1 (-)\boldsymbol{n}_2)$. They consist of in- and outgoing straight interfaces of orientations $\boldsymbol{n}_1$ and $\boldsymbol{n}_2$ with possibly a part or a sequence of intersecting parts of the $\boldsymbol{QR}$ curve as a connection. Note that a $C(\boldsymbol{n}_1 (+)\boldsymbol{n}_2)$ shape can in principle only contain convex parts of the $\boldsymbol{QR}$ curve and a $C(\boldsymbol{n}_1 (-)\boldsymbol{n}_2)$ shape only concave parts. So we might say that in the case of the protruding edge we have to deal with a convex point source in the origin and in a re-entrant edge with a concave point source. This implies that, for the sake of defining a construction algorithm, we can neglect the nonapplicable parts of the $\boldsymbol{QR}$ curve beforehand in order to simplify the procedure. This can be generalized to the 3D case, and can greatly simplify the 3D algorithm too.

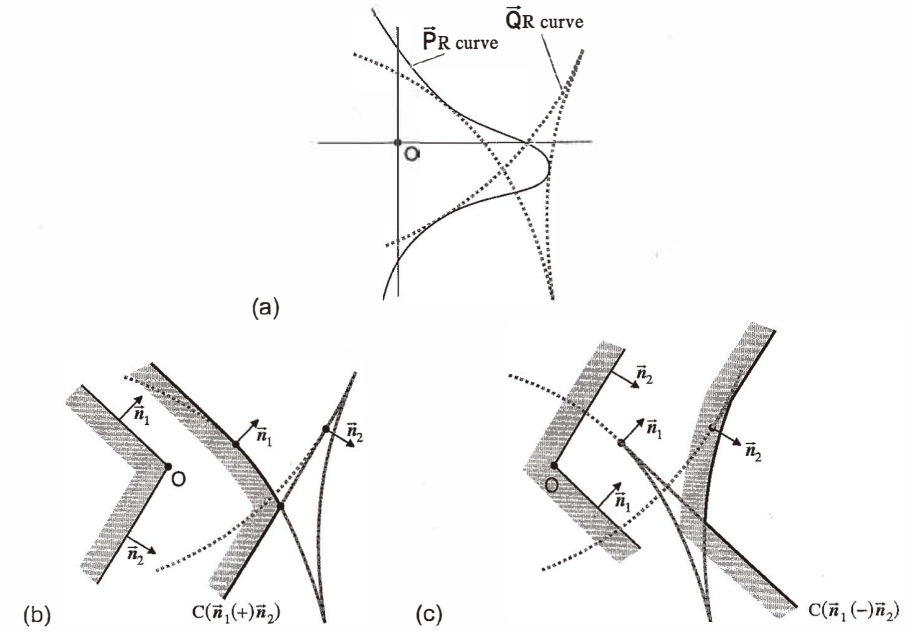

Fig. 4. Evolution of protruding vs re-entrant edge (2D case). a) ***PR*** and ***QR*** curves = point of departure for evolution construction, b) Case of protruding edge. c) Case of re-entrant edge.

5. The 3D Case: Evolution of Vertices.

Whereas the "elements" in the 2D starting edge were 1) the two edge legs (= half-infinite lines) and 2) the edge point, we have in the 3D 3-vertex case, for any of the eight vertex types, to deal with three kinds of elements in the starting shape:

1) Three planar elements (sectors of infinite planes, each defined by two of the three half-line edges),

2) Three half-line elements (edges, meeting in the vertex),

3) One point element (vertex point).

At time $t = 0$, each of these types starts moving and evolving into a specific type of surface, characterized by its specific curvature type. In the same order, we obtain

1) From the three sector elements: the same sectors, each displaced by their appropriate $\boldsymbol{QR}(\boldsymbol{n}_i)$ vector,

2) From the three half-infinite edges: a combination of cylindrical and eventually conical surfaces (see below, section 5.1) and,

3) From the vertex point: the doubly curved part(s) of the $\boldsymbol{QR}(\boldsymbol{n})$ surface evolving from the triangle of orientations between $\boldsymbol{n}_1$, $\boldsymbol{n}_2$ and $\boldsymbol{n}_3$ latently present in the protruding, re-entrant or saddletype point source, with the appropriate curvatures (see below, section 5. 2).

All surfaces overlap or are connected at their boundaries, together forming a sheet extending to infinity in all directions. The sheet as a whole can have self-intersections. All parts of the surface beyond such self-intersections are nonphysical and have to be eliminated. The evolution shape is the surface that survives after this elimination. It is the 3D analog of the 2D $C(\boldsymbol{n}_1\,(\pm)\boldsymbol{n}_2)$ curve and we will call it the $S(\boldsymbol{n}_1\,(\pm)\boldsymbol{n}_2\,(\pm)\boldsymbol{n}_3\,(\pm))$ surface, which is defined in 3D velocity space.

5.1 *Cylindrical and conical areas*

Cylindrical surfaces are defined as ruled surfaces, in this case defined by lines parallel with the edge. The radius in the edge direction is infinite. Conical surfaces are also ruled surfaces (with one infinite radius), but the describing lines all pass through the vertex (= cone apex). The cylindrical part is sufficiently clear and it corresponds to the curve $\boldsymbol{QR}(\boldsymbol{n})$ for $\boldsymbol{n}$ following the great arc from $\boldsymbol{n}_i$ to $\boldsymbol{n}_k$. The construction is identical to that in section 4: we have to choose between the concave and the convex part of this $\boldsymbol{QR}(\boldsymbol{n})$ curve, in accordance with the sign of the edge. Whereas this curve is a line curve in 3D velocity space, the cylindrical surface is defined by extending every point of it to infinity in the direction of the edge. For an edge that is infinite in both directions, the cylindrical surface also extends to both sides. In contrast, in our 3D-vertex case we have to deal with a half-infinite edge line and thus the cylindrical surface only extends in one direction from the vertex. All points of this cylindrical surface correspond to kinematic wave trajectories which have started from a point on the edge at $t = 0$.

The conical part, if it occurs, is related to the possibility that the moving endpoint (= vertex point) continuously adds new length to the edge. This is illustrated schematically in Fig. 5 where we have chosen a 2D $\boldsymbol{QR}$ curve resembling that in Fig. 4 as a point of departure (see insert). This is the case if $\boldsymbol{R}_{\text{vertex}}$ is directed beyond the spatial area defined by the half-cylindrical part. A conical part is then generated (in the opposite case it is occluded by the half-cylindrical part). Points on the conical part have started later, at $t > 0$, simply because the edge had not yet reached the corresponding position at $t = 0$. As the endpoint of the edge moves at a constant speed along a straight trajectory, this endpoint emits kinematic wave trajectories continuously, i.e., for that conical surface it acts as a velocity source.[14,16] Correspondingly, the shape of the cone can be calculated by the conical Gibbs-Wulff construction, which describes the cone shape induced by a velocity source (see appendix and Ref. (9)).

It is a consequence of this construction that the surface defined by the connected cylindrical plus conical areas has a saddletype character. This can be seen in Fig. 5 (the sign of the corner between connected ruling lines on cone and cylinder is opposed to the curvature in the other direction). This applies to protruding as well as re-entrant edges. This saddletype character as such is sufficient proof that a conical area cannot occur in the evolution shape of either a protruding or a re-entrant vertex in principle. However, for the saddlepoint case conical areas can survive, because such vertices are meeting points of re-entrant and protruding edges.

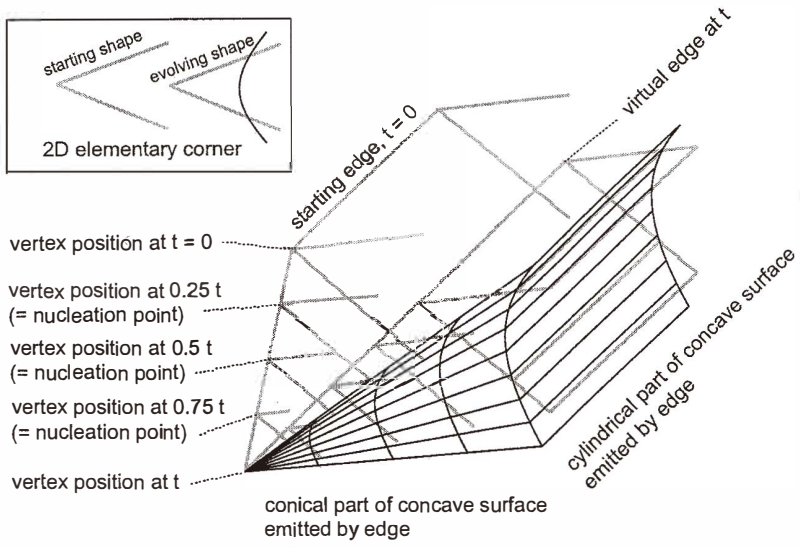

Fig. 5. Cylindrical and conical areas as emitted by the line source of a half-infinite edge whose endpoint follows a trajectory diverging from the cylindrical area. The example shows a re-entrant edge similar to the 2D case sketched in Fig. 4(c).

5.2 *Areas with double curvature*

In the discussion of the 2D case we emphasized the identification of protruding edges with convex line sources and of re-entrant edges with concave line sources, instead of the conventional identification of protruding edges with the survival of slow orientations, and of re-entrant edges with the survival of fast orientations. In the 3D case, this conventional identification works for protruding and re-entrant vertices, but it gives no clue for the handling of saddlepoint vertices. Here we see the advantage of the alternative identification: recognizing the saddletype of the involved point source, we can exclude convex as well as concave parts of the ***QR*** surface, and even those saddletype parts whose curvatures do not correspond to the starting saddlepoint vertex. Note that concave and saddletype regions do not necessarily occur in a ***QR*** surface. If not, we can reduce the intersection calculations for re-entrant edges and re-entrant and saddletype vertices by neglecting the ***QR*** surface altogether.

Note that the elimination of the nonapplicable parts of the ***QR*** curve/surface (= those parts with the inappropriate curvature) is not really necessary for the construction to succeed. Rather it is an intuitive aid in understanding which parts of the ***QR*** curve/surface participate in the end result. As can be seen in the construction procedure of Figs. 4(b) and 4(c), the inapplicable parts of ***QR*** are eliminated automatically in the 2D case. The same happens in the 3D construction. However, depending on the ear-cutting procedure used, eliminating them beforehand can reduce the complexity of the ear-cutting algorithm and therefore the computing time as well.

5.3 *The 3D construction procedure in one or two steps*

Now that all surface types that can participate have been mentioned, we may proceed to develop the construction procedure for the evolution shape of a vertex. We emphasize that this procedure involves a single step for a re-entrant or a protruding vertex, but two steps for a saddlepoint vertex.

In the first step the surface $S(\boldsymbol{n}_1\,(\pm)\boldsymbol{n}_2\,(\pm)\boldsymbol{n}_3\,(\pm))$ is determined, but without the conical areas. We call this surface $S^{(1)}(\boldsymbol{n}_1\,(\pm)\boldsymbol{n}_2\,(\pm)\boldsymbol{n}_3\,(\pm))$. For protruding and re-entrant starting vertices, this first step is already sufficient, because we know beforehand that S cannot include conical areas in any case, and therefore $S^{(1)}$ and S coincide (see section 5.2).

For saddletype starting vertices, however, the surface $S^{(1)}$ may have one or more (moving) saddlepoint vertices. If so, these moving saddlepoint vertices may still appear in the final surface S, but eventually they may have an additional, nucleated, conical area. This has to be checked, and the shape of the conical area determined, by the "conical Gibbs-Wulff construction": this is the second step of the procedure (this second step has to be worked out for all saddlepoint vertices occurring in $S^{(1)}$).

Because one of the input data required for the conical Gibbs-Wulff construction is the vertex velocity $\boldsymbol{R}_{\text{saddlepoint vertex}}$ of the saddlepoint vertex under consideration, it is now evident why we could not combine this construction directly with step 1. $\boldsymbol{R}_{\text{saddlepoint vertex}}$ is a result of the "step 1" procedure, so it is only available afterwards. All vertices found in $S^{(1)}$ are trajectory-persistent, and their vector velocity is not affected by eventual conical areas nucleated by them: thus, their $\boldsymbol{R}_{\text{saddlepoint vertex}}$ vectors are correct input data for the conical Gibbs-Wulff construction.

The result of the second step (i.e., the conical Gibbs-Wulff checks for all saddlepoint vertices occurring in $S^{(1)}$) is a list of $n \geq 0$ newly discovered conical areas. These do not occur in $S^{(1)}$, and therefore we have to amend the preliminary evolution shape $S^{(1)}$ in order to take them into account. The result of this amendment —again after elimination of the (new) self-intersections— is called $S^{(2)}$. This surface $S^{(2)}$ may contain new saddlepoint vertices as compared with $S^{(1)}$, which have to be checked again. This iteration continues, until new saddlepoint vertices are no longer found. The new vertices found in each of the surfaces $S^{(1)}$, $S^{(2)}$, *etc.* may be labeled as belonging to the first, second, and so on "generations" of vertices. Altogether, in this way, in principle we have to follow a chain of a finite number of cycles, each of which yields a new generation of conical areas and vertices. These generations are linked in a causal chain, which is to be followed until new vertices are no longer detected. We emphasize that, although we have to work our way through a list of "steps 2" which may be longer or shorter (≥ 0 checks), the shape of the structure is still predictable in a single time step.

6. Explanation of the Underetched Convex Mask Corner on {100} Silicon

The structure of the underetched convex mask corner on {100} silicon has a certain reputation because of its complexity. The case was investigated in detail by Schröder and Obermeier[7] and Schröder[8] for various compositions and temperatures of KOH and TMAH etchants. Different etch conditions result in different structures, and the nucleating

saddlepoint vertices which are the focus of interest in this paper are not always present. They are not an inevitable consequence of the saddletype point source character of the convex mask corner, as the etch rate function also has to satisfy certain conditions. The structure shown in Fig. 1 (courtesy H. Schröder) was etched in pure KOH/H_2O solution (33wt%. 80°C) and shows a complex shape involving ten vertices in three generations. We chose this example to illustrate the principles developed above.

The starting situation is sketched in Fig. 6(a). The mask edges are aligned along the <110> and <10> directions. The first generation, i.e., without the conical areas, is obtained by intersecting surfaces of types 1, 2 and 3 as referred to in section 5, but still without the conical sections emerging from the edge endpoints ("step 1" of the two-step procedure of section 5).

Ad 1) With respect to the three planar sectors involved, only one is relevant: the (100) plane in the 270° exposed sector between the <110> and the <110> edges. Its ***QR*** direction is vertically downwards.

Ad 2) The cylindrical surfaces starting from the mask-edge line sources are the almost-planar {111} surfaces whose etching speed is very low. In practice, $R(111)/R(100)$ may be as low as 0.01, but in order to make it clear that the velocity is not zero we have exaggerated $R(111)$ in Fig. 6(b) to a visible value. In Figs. 6(b), 6(c) and 6(d) these surfaces are the trapezoids $B_1A_1D_1C_1$ and $B_2A_2D2_2C_2$.

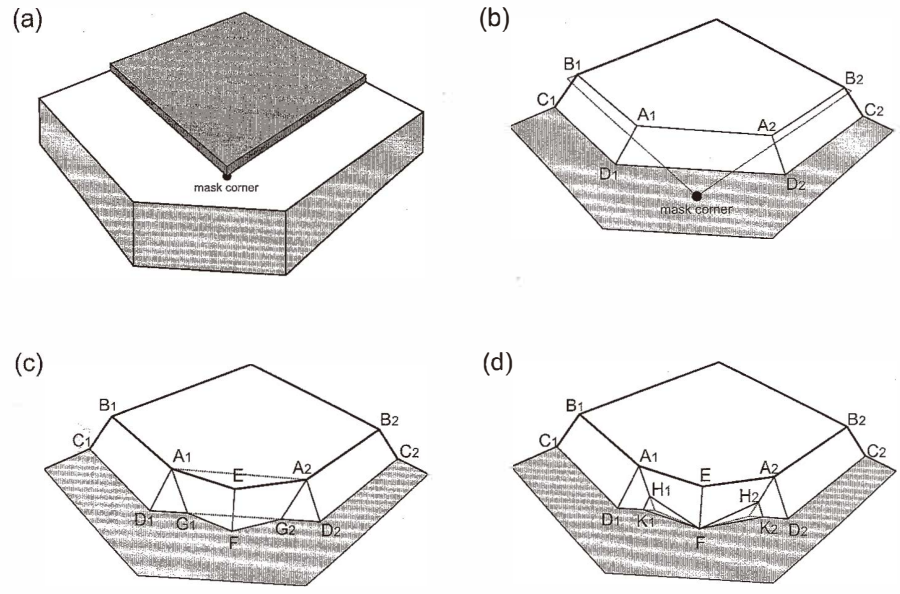

Fig. 6. The three stages of construction of the underetch shape following the algorithm for the saddlepoint vertex. a) Initial shape. b) "First generation", before checking procedure by conical Gibbs-Wulff construction. c) Addition of four conical sectors found by checking points A1, A2, D1 and D2. d) Addition of two conical sectors found by checking the new point F, resulting from step c).

Ad 3) Finally, the doubly curved $\boldsymbol{QR}(\boldsymbol{n})$ shape emerging from the origin (mask corner) should have the appropriate saddletype curvature. The orientations obeying this condition are the (110) orientation and a vicinal region near (100) tilted towards (110). In Fig. 6(b), the (110) area corresponds to the trapezoid $A_1A_2D_1D_2$ (at 45° with the mask). The triangular region $D_1M^*D_2$, where M* is the projection of the mask corner onto the receding (100) plane, may correspond to the vicinal region near (100), but this identification is uncertain because the difference with the surrounding exact (100) area is hardly detectable (see below).

Thus, roughly speaking (i.e., approximating all surfaces by planes), the first-generation surface consists of the assembled (100), (110), (111) and (111) planes, each displaced by their $\boldsymbol{QR}$ vectors and connected in their intersections (Fig. 6(b)). This surface has four saddlepoint vertices A_1, D_1, A_2 and D_2. A_2 and D_2 are mirror images of A_1 and D1, respectively. The second step in the procedure (section 5) is to check whether the conical Gibbs-Wulff construction predicts the nucleation of a conical bevel area for the vertices A_1/ A_2 and for D_1 /D_2.

Looking now at the experimental structure, we can observe that the points A_1 and A_2 do exhibit a 4-plane vertex. Consequently we conclude (based on this observation only) that a cone is nucleated, and we can also identify the nucleated cones as the planes A_1EFG_1 and A_2EFG_2, because the latter are new as compared to the first generation structure. The cones are almost planar (in agreement with a "sharp" saddlepoint in the $\boldsymbol{PR}(\boldsymbol{n})$ surface), and their orientation is approximately {411}. The new saddlepoint vertices formed by the second generation are E and F, which each have to be checked again for nucleating activity of a next generation of conical areas.

The points D_1 and D_2 are also saddlepoint vertices and might in principle nucleate a conical area. The triangular region $D_1M^*D_2$, being in the shadow of the mask, cannot in principle have exact (100) orientation because it is not etched directly from above. On the other hand, in the experimental structure of Fig. 1, the difference between this triangle and the exact (100) surroundings is hardly visible. In precision measurements by Schröder[9] it was found that the etch depth at point F was actually about 4% less than that of the (100) plane. In the present discussion we will neglect the details of this triangular area $D_1M^*D_2$, because they are hardly visible anyhow. Certainly, we cannot distinguish between the options a) that the region corresponds to a saddletype doubly curved $\boldsymbol{QR}$ surface evolving from M, or b) that it is composed of two conical areas nucleated from D_1 and D_2, as would also be possible. In agreement with this, we have omitted the point M* from the sketches in Fig. 6 and we have depicted the triangle $D_1M^*D_2$ as being identical with the surrounding (100) area.

Continuing the analysis, we find from the experimental structure that saddlepoint vertex F nucleates two (symmetrically equivalent) conical sections, FH_1K_1 and FH_2K_2. These are clearly the result of the second round of "step 2" procedures. Again the cone areas are nearly planar, now with orientation roughly {441}. Clearly the saddlepoint vertex E is shape-persistent. The newly formed vertices H_1, K_1, H_2 and K_2 are all protruding and do not need to be checked. This automatically brings the construction algorithm to its conclusion.

Summarizing the entire procedure, we can recognize the underlying causal chain of nucleating saddlepoint vertices, linked by nucleated conical sections: area $A_1A_2D_1D_2$,

saddlepoint vertices A_1+A_2 → areas A_1EFG_1 and A_2EFG_2, new saddlepoint vertices E and F → areas FH_1K_1 and FH_2K_2 (end). The resulting structure contains three nucleating saddlepoint vertices, three shape-persistent saddlepoint vertices and four protruding vertices, together defining ten areas.

We have to emphasize that our explanation of this structure, including the connectivity of the causal chain, is deduced from the experimentally observed structure. It has not yet been checked by starting from the $R(\boldsymbol{n})$ function and performing all steps of the construction algorithm numerically, as would be possible. However, we feel that the correspondence between the chain of >3-edged saddlepoint vertices and the experimental structure is sufficiently strong evidence for our explanation, at least as far as the principle is concerned.

We emphasize that the structure discussed here was chosen to illustrate the principles of saddlepoint evolution. It is certainly not representative for all structures that can be obtained for the same substrate orientation and mask configuration by etching at different temperatures and/or etchant compositions. The experiments by Schröder[9] show clearly that even slightly different conditions may give rise to significantly different geometries, some even without nucleating saddlepoint vertices at all, *e.g.*, for KOH with addition of isopropyl alcohol (IPA). Also Lee[17] published a structure for the same crystallographic situation (Si and mask orientation), but hydrazine/IPA as the anisotropic etchant, which has only regular 3-edged saddlepoint vertices composed of {211} oriented surfaces. This is hardly a surprise: we can see in Fig. 1 that some of the surfaces that produce the structure of Fig. 6(d) by mutual intersection differ only slightly in orientation. A small change in the shape of the $R(\boldsymbol{n})$ function may therefore markedly affect the relative positions of the intersections, and consequently the shapes themselves.

7. Conclusions

The observation of saddlepoint vertices connecting more than three edges and planes in a crystal surface during growth or dissolution is geometrical proof that one or more of the planes is nucleated by the presence of the others in the saddlepoint vertex. This concept has been developed in the terminology of (3D) kinematic wave theory. We have shown that the phenomenon is a straightforward consequence of the principles of kinematic wave theory, although this appears to have remained unnoticed to date. The structures developing from any given initial shape can be predicted by an algorithm based on this theory. For an arbitrary single vertex, including the saddletype case, this can be done in a single time step.

The phenomenon is of technical importance in the wet-chemical etching of crystals such as silicon and quartz for the fabrication of microdevices. Experimentally observed structures of the underetched convex mask corner on Si(100) can be fully understood on the basis of our algorithm.

The algorithm for saddletype vertex simulation requires an extra step as compared with that for a convex or a concave vertex. This extra step completes the toolbox required for numerical simulation of the evolution of arbitrary 3D shapes.

Acknowledgements

The experiments by H. Schröder were an important source of inspiration for this analysis. We acknowledge his permission to use his SEM image in Fig. 1. This work was supported by the Dutch Technology Foundation (STW).

References

1 F. C. Frank: Growth and Perfection of Crystals (John Wiley, New York 1958) p. 411.
2 A. A. Chernov: Sov. Phys. Crystallography **8** (1963) 401.
3 I. V. Katardiev, G. Carter, M. J. Nobes, S. Bay and H. O. Blom: J. Vac. Sci. Technol. A **12** (1994) 61.
4 C. H. Sequin: Sensors and Actuators A **34** (1992) 225.
5 J. S. Danel and G. Delapierre: Sensors and Actuators A **31** (1992) 267.
6 H. K. Trieu and W. Mokwa: J. Micromech. Microeng. **8** (1998) 80.
7 H. Schröder and E. Obermeyer: J. Micromech. Microeng. **10** (2000) 163.
8 H. Schröder: "Modell des anisotropen Ätzens von einkristallinem Silizium in wäszrigen KOH-Lösungen", Thesis, Berlin 2000.
9 J. van Suchtelen and E. van Veenendaal: The role of saddlepoint vertices in the kinematic wave theory of growth and dissolution of crystals, Phys. Rev. B, submitted.
10 R. Kern: Morphology of Crystals A, ed. I. Sunagawa (Terrapub, Tokyo, 1987) Chap.2.
11 P. Bennema and G. H. Gilmer: Crystal Growth, an introduction, ed. P. Hartmann (North-Holland, Amsterdam/London 1973) Chap. 10, p. 310.
12 D. W. Shaw: J. Cryst. Growth **47** (1979) 509.
13 R. J. Jaccodine: J. Appl. Phys. **33** (1962) 2643.
14 J. van Suchtelen, A. J. Nijdam, J. G. E. Gardeniers, M. Elwenspoek, E. van Veenendaal, W. J. P van Enckevort and E. Vlieg: Generalisation of the kinematic wave theory to growth and dissolution of imperfect Crystals, Phys. Rev. B, submitted.
15 J. van Suchtelen, A. J. Nijdam and E. van Veenendaal: J. Cryst. Growth **198–199** (1999) 17.
16 J. van Suchtelen: Morphology of Crystals C, ed. I. Sunagawa (Terrapub, Tokyo, 1995).
17 D. B. Lee: J. Appl. Phys. **40** (1969) 4569.

APPENDIX: the conical Gibbs-Wulff construction

All conical interfaces which are nucleated by a moving saddlepoint vertex acting as a velocity source during the etch process necessarily obey eq. (1), the connectivity relation, which expresses that the surface oriented at $\boldsymbol{n}$ keeps pace with the vertex. This implies that the orientations of these interfaces can be found from the intersection of the polar plot $\boldsymbol{PR}(\boldsymbol{n})$ and the sphere $\boldsymbol{P}[\boldsymbol{R}_{\text{vertex}} \bullet \boldsymbol{n}]$. We call this intersection the conecurve of Rvertex.

We define the baseplane of Rvertex as the plane through the origin perpendicular to Rvertex. The conecurve of Rvertex can be projected onto this baseplane from the point Rvertex. The projected curve can be considered as the polar plot for the orientation-dependent advance rate $R^{(2)}$ of the intersections of cone planes with the baseplane, $\boldsymbol{P}^{(2)}R^{(2)}(\boldsymbol{n}_{\text{proj}})$. Here $\boldsymbol{n}_{\text{proj}}$ is the normal of the intersection line in the baseplane, and $\boldsymbol{P}^{(2)}$ is used as a symbol for the 2D $\boldsymbol{P}$ operator defined in the baseplane. By analogy with the

Gibbs-Wulff construction for shapes generated by a point source, the actual intersection of the cone areas nucleated by the velocity source and the baseplane correspond with the relevant sections of the shape $\boldsymbol{Q}^{(2)}R^{(2)}(\boldsymbol{n}_{\text{proj.}})$ as cut off by the edge sections. The cone area itself is formed as the surface obtained by connecting this curve with the apex Rvertex. Consequently we call this the conical Gibbs-Wulff construction for the cone shape.

In the first step of the two-step procedure discussed in section 5, we find moving saddlepoint vertices without conical areas. Such a vertex is trajectory-persistent, i.e., its existence and trajectory is fixed by $\boldsymbol{n}_1$, $\boldsymbol{n}_2$ and $\boldsymbol{n}_3$ which can be determined from the evolution shape as found in the first step, and its vector velocity is therefore = $R(\boldsymbol{n}_1,\boldsymbol{n}_2,\boldsymbol{n}_3)$. The planes $\boldsymbol{n}_1$, $\boldsymbol{n}_2$ and $\boldsymbol{n}_3$ participate in the vertex. In Fig. 7(a) we have depicted such a saddlepoint vertex $[\boldsymbol{n}_1\,(-)\boldsymbol{n}_2\,(+)\boldsymbol{n}_3\,(-)]$ schematically, still without conical areas, as an example. The intersections of the sectors with the baseplane can be drawn, they are indicated as $\boldsymbol{n}_2$ and $\boldsymbol{n}_3$ in Fig. 7(b). The mutual intersection points of Np and Nq are

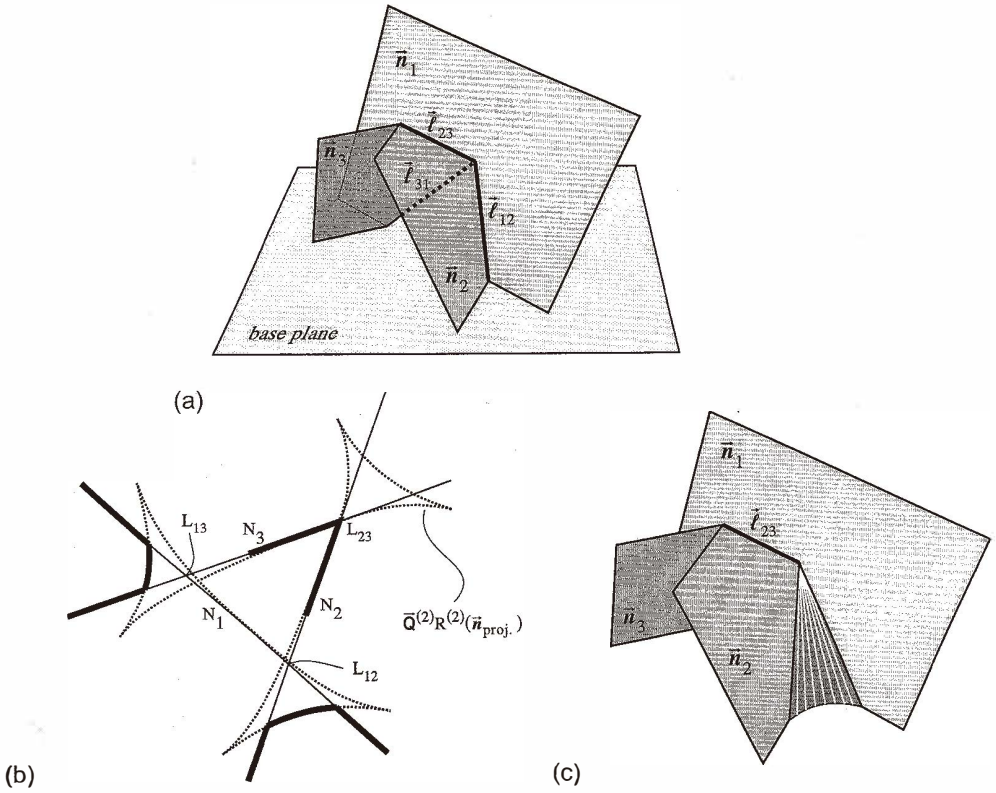

Fig. 7. Illustration of conical Gibbs-Wulff construction for a saddlepoint vertex. a) Saddlepoint vertex $[\boldsymbol{n}_1\,(-)\,\boldsymbol{n}_2\,(+)\,\boldsymbol{n}_3\,(-)]$ without conical areas, moving upwards + base plane. b) Conical Gibbs-Wulff construction for the conical areas nucleated by the moving vertex point, as drawn in the base plane. c) Resulting structure.

indicated as L_{pq}. We have chosen a $\boldsymbol{Q}^{(2)}R^{(2)}(\boldsymbol{n}_{\text{proj.}})$ curve which produces conical areas in the re-entrant edges. In Fig. 7(b) the character of the edges shows up in the points L_{pq}. L_{23} represents a protruding edge, whereas L_{12} and L_{13} represent re-entrant edges. Each of the edges in the baseplane evolves according to the method illustrated in Figs. 4(b) and 4(c). Correspondingly, the conical areas can be found from the eventually beveling curves found for the three edges in the baseplane, by forming the corresponding cones to the vertex point. A perspective view of the resulting persistent structure of the saddlepoint vertex is sketched in Fig. 7(c).

We emphasize that the use of Fig. 7 to illustrate the principle of the conical Gibbs-Wulff construction should not be considered to imply that a nucleated cone is always a faster area in a re-entrant edge. By the same procedure, a slower conical area can be constructed in a protruding edge of a saddlepoint vertex. This is the case in the experimental structure analyzed in section 6.